Coating Strain Induced Distortion in LIGO Optics

Kartik Srinivasan

Research Supervisor: Dennis Coyne

Faculty Sponsor: Professor Rochus Vogt

Abstract:

LIGO (Laser Interferometer Gravitational Wave Observatory) core optics are coated with multilayer dielectric (SiO_2/Ta_2O_5) coatings through ion beam sputter (IBS) deposition. An IBS deposited coating is under compressive strain due to its high density, and this strain causes a deformation in the substrate. Very stringent surface figure requirements are necessary for LIGO to detect gravitational waves, and thus, it is important to study such aberrations in the optics. This was done through analytical and finite element models. The analytical model used Kirchoff thin plate theory to predict the strain induced deformation and provide an approximate analysis of the situation. The finite element models accounted for the three-dimensional elasto-static response of the mirror and included factors that were neglected in the analytical approach (such as edge effects and a thick plate response), thus providing a more accurate picture of the problem. Both models were used to predict deformation for fused silica (initial LIGO) and sapphire (possible future LIGO) optics. The results obtained from these analyses provide estimates for the radius of curvature changes in LIGO optics due to coating strain induced distortion.

Introduction:

-Introduction to LIGO

The Laser Interferometer Gravitational Wave Observatory is a collaborative effort between Caltech and MIT scientists aimed at the first direct detection of gravitational waves. Einstein's general theory of relativity predicts the existence of gravitational waves, and this prediction has been indirectly confirmed (through observations of pulse arrival times of the binary pulsar PSR 1913+16) by radio astronomers, but it has never been verified through direct detection. Should LIGO succeed in its goals, not only will it provide the first such detection, it will also provide a new method of observing the behavior of astronomical objects such as black holes.

To detect gravitational waves, LIGO employs laser interferometry. A very simple explanation of how a Michelson interferometer can detect gravitational waves is as follows. Gravitational waves interact with matter in such a way that they expand it in one direction and compress it in the orthogonal direction. Hanging mirrors (that can only move in one direction) are placed in the configuration below (Figure 1), and a laser beam is sent through the beamsplitter down the two arms of the interferometer. The light reflects within the arms several times (each arm is a Fabry-Perot cavity) before interfering, at which point the interference pattern is picked up by the photodetector. If a gravitational wave had passed, one arm would have increased in length by an amount ΔL, while the other arm would have decreased in length by ΔL. The differing lengths would have caused the light from the two arms to be out of phase, thus producing an interference pattern when the light recombines (if no gravitational wave had passed, the light would remain in phase). The sensitivity required is proportional to the strain $\Delta L/L$ (where L is the arm length), so if all else remains equal, longer arms facilitate detection. Even with four kilometer long arms, the initial goal for LIGO is to detect a displacement of 10^{-18} m.

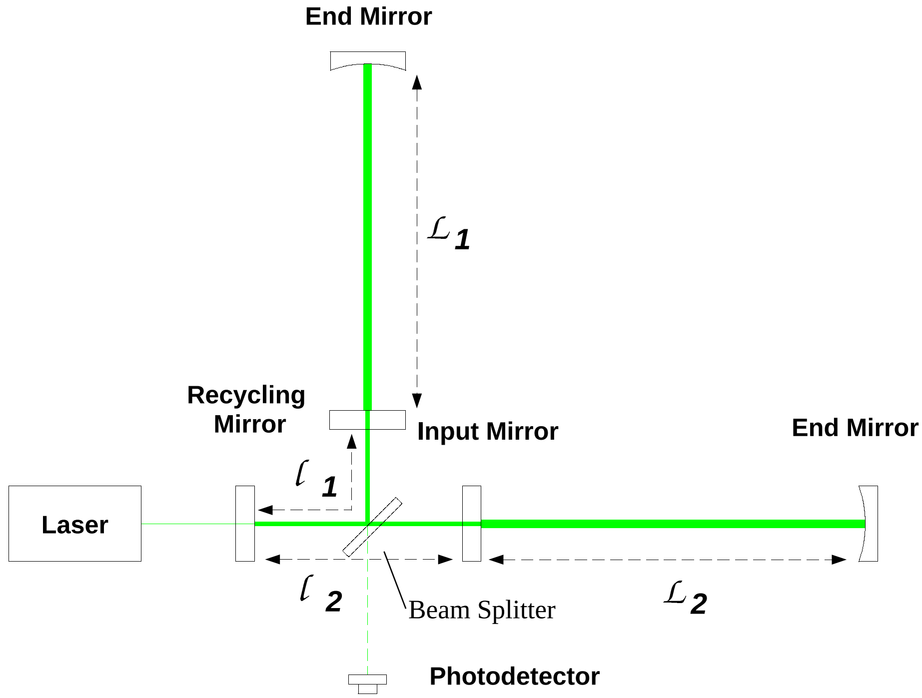

FIGURE 1. Basic Configuration of a LIGO Interferometer. LIGO Interferometers will exist in two sites. One is in Hanford, Washington, while the other is in Livingston, Louisiana.

To achieve the precision necessary to measure such a small displacement, LIGO's optics must be of the highest quality. A completed optical component must maintain a very precise surface figure (λ</800) and have a radius of curvature equal to the prescribed value up to nearly a part in 100. It is therefore very important to investigate possible sources of distortion. One such source is coating strain induced deformation in the optics. Before discussing such deformation, a brief review on coating strain is given.

-Coating Strain

A deposited optical coating is more than likely under a certain amount of stress (and therefore strain). This stress can either be tensile or compressive, and is in general composed of two major components. The first components is a thermal stress that arises from the unequal thermal contractions of the substrate and its coating [1]. A coating is typically deposited at a higher temperature than what the stress is measured at, and thus, when the coating and substrate cool, they do so unequally due to their differing coefficients of thermal expansion. Depending upon the relative magnitudes of these coefficients, a state of compressive strain or tensile strain will evolve. The second component of the total strain is a growth strain (sometimes referred to as an intrinsic strain) that arises because the density of the deposited film might be greater or less than its ideal state. LIGO optics are coated by a process called ion beam sputtering (IBS), which is schematically shown below. IBS coated optics are almost exclusively under compressive stress [2]. Theories exist explaining why compressive stress forms and which deposition process parameters affect it. Before moving further, these theories will be briefly reviewed.

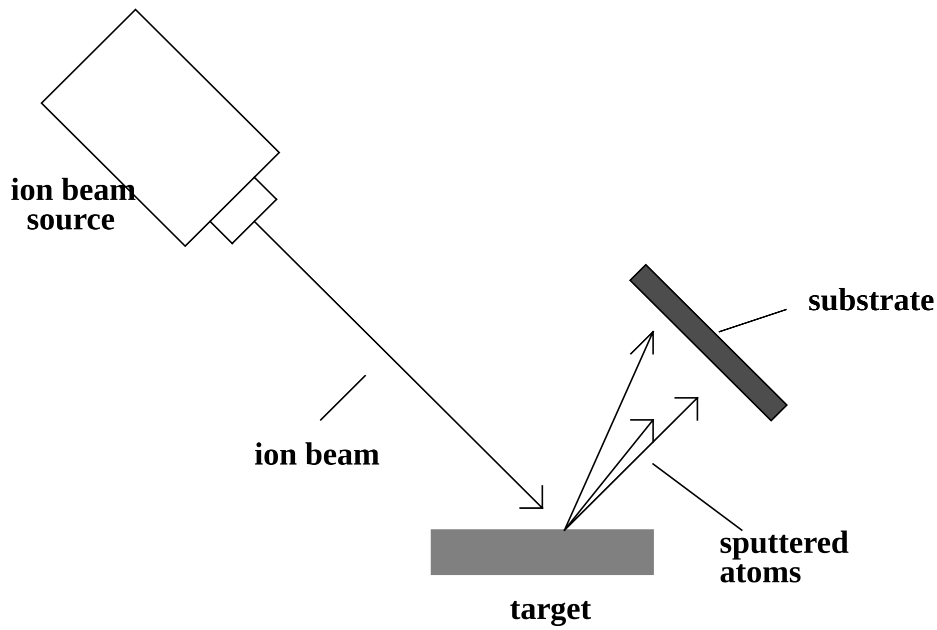

FIGURE 2. Schematic Diagram of a typical ion beam sputtering apparatus. Very simply, the ion beam knocks atoms off the target (which is usually made of the substance that is to comprise the coating) and on to the substrate.

The two predominant theories that explain the formation of compressive stress are the impurity model and the atomic peening (forward sputtering) model [2]. The impurity model is based on the idea that lattice distortion in a film is produced by the existence of atoms (molecules) of a different size than the size of the film molecules. Some common impurities are oxygen, water vapor, hydrogen, and noble gases (which are the sputtering gases). Experiments have shown that increasing the pressure or concentration of such molecules in the deposition process increases the amount of compressive stress (or decreases the amount of tensile stress). However, no models exist that quantitatively explain these phenomena [2].

The forward sputtering model attributes compressive stress to the interaction of energetic particles with the growing film. The collisions produce distortions in the film, and these distortions evidence themselves as compressive strain. Quantitative models for this process *have* been produced, and these models give some explanation as to how deposition parameters affect the stress. In particular, it is believed that stress (as stated above) is a function of the microstructure of the film, which in turn is determined by the energies (thermal and kinetic) of the deposition process. Some of the basic process parameters which can affect these energies are pressure, the ratio of target atom mass to sputtering atom mass, substrate orientation, and temperature [2]. Specific relationships between stress and some of these parameters have been developed (they will not be discussed in detail); for example, an inverse relationship between deposition temperature and intrinsic stress has been shown experimentally. Thus, to a limited extent, the amount of stress that exists in a film can be controlled if the process parameters can be changed without compromising the quality of the film.

-Coating Strain Induced Distortion

Having accepted that the coatings for LIGO optics will be under compressive strain, it follows that the associated substrates (the mirrors) will be distorted. Qualitatively, the distortion arises because a film under compressive stress would like to expand but can not because it is being restrained by the substrate. Thus, the stress has a tensile effect on the substrate, causing it to bow outwards in a convex shape. This distortion will affect the radius of curvature of the optic, and it is the objective of this paper to determine to what extent (approximately) the radii of curvature of the optics will change.

-Strength of Materials Solution

G.G. Stoney published a paper that addresses the situation in terms of a two-dimensional beam [3]. His formula was expanded by R.W. Hoffman to make it applicable to plates[4]. Hoffman’s approach uses Kirchoff thin plate theory and thus provides only an approximate analysis for the case at hand. The reason for this is that thin plate theory is based upon the assumption that the aspect ratio (the ratio of length to height in a two dimensional case) of the substrate is large, and the substrate is therefore a thin plate. In the LIGO case, this is not necessarily true (the aspect ratio for an End Test Mass is only 2.5). Nevertheless, the solution is still valuable for providing estimates and a check on further analyses. The analyses found in these papers, as well as in [5], are briefly summarized below.

Begin with a substrate of thickness t_s, elastic modulus E_s, Poisson’s ratio v_s, and radius of curvature R (which is induced by the coating stress) that is coated by a film of thickness t_f. The biaxial modulus for the substrate is then $E_s/(1-v_s)$ (the biaxial modulus is effectively what extends the beam theory analysis, which just uses the elastic modulus, to the plate theory analysis). If b is the depth from the surface to the neutral axis (neglecting t_f since $t_f \ll t_s$), then

$$\int_{t_s}^{0} \frac{E_s}{R(1-v_s)}(b-x)x\,dx = 0$$

because the sum of the moments about the neutral axis must be zero. Dividing through by the constants and solving this integral gives the following result

$$-\left[\frac{t_s^2}{2}b - \frac{t_s^3}{3}\right] = 0 \rightarrow b = \frac{2t_s}{3}$$

If σ is the stress in the film, then

$$\sigma t_f = \int_{t_s}^{0} \frac{E_s}{R(1-v_s)}(b-x)dx$$

$$\sigma t_f = \frac{E_s}{R(1-v_s)}\left(\frac{t_s^2}{2} - bt_s\right)$$

$$|\sigma| = \frac{E_s t_s^2}{6R(1-v_s)t_f}$$

From Hooke's Law,

$$\sigma = \frac{E_f}{(1-v_f)}\varepsilon$$

where ε is the strain and E_f and v_f are the elastic modulus and Poisson's ratio of the *film*. Substituting in for the stress and solving in terms of the curvature K=1/R gives

$$K = \frac{6E_f(1-v_s)t_f}{E_s(1-v_f)t_s^2}\varepsilon$$

Finally, the deflection can be related to the curvature geometrically if one considers the following picture, where r is the radius (or half the length) of the substrate, δ is the deflection, and R is the radius of curvature.

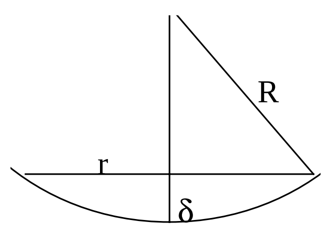

FIGURE 3. Geometrical Diagram for Calculating Curvature from Deflection

From geometry

$$\delta(2R-\delta) = r^2 \rightarrow \delta = R - R\sqrt{1 - \frac{r^2}{R^2}}$$

Taking the first-order Taylor's expansion of the radical term gives

$$\delta = \frac{r^2}{2R} = \frac{1}{2}Kr^2$$

From this, one can calculate the expected deflection given a coating stress and the mechanical constants of the film and substrate.

However, LIGO optics have multilayer coatings (the exact physical specifications will be given later), so the above analysis is incomplete. Rather than extend the analysis for multilayer films, the multilayer coatings are treated as single composite coatings. This is made easier by the fact that LIGO coatings contain only two types of films (SiO_2 and Ta_2O_5). Thus, even though a LIGO coating may have multiple layers, layers of the same material are combined into a single layer in the analysis. Using composite theory [6], an effective elastic modulus and Poisson's ratio (denoted by the subscript *eff*) for the coatings is calculated. In the analysis below, a numbered subscript *i* denotes film *i*.

$$A^{\prime} = \frac{E_{eff}}{1 - v^2_{eff}} = \left(\frac{1}{\sum_i t_i}\right)\sum_i \frac{t_i E_i}{1 - v^2_i}$$

$$B^{\prime} = \frac{v_{eff} E_{eff}}{1 - v^2_{eff}} = \left(\frac{1}{\sum_i t_i}\right)\sum_i \frac{t_i v_i E_i}{1 - v^2_i}$$

Solving for v_{eff} and E_{eff} gives

$$v_{eff} = \frac{t_1 v_1 E_1\left(1 - v_1^2\right) + t_2 v_2 E_2 (1 - v_2^2)}{t_1 E_1 (1 - v_2^2) + t_2 E_2\left(1 - v_1^2\right)}$$

$$E_{eff} = \frac{E_1 t_1 + E_2 t_2}{t_1 + t_2}$$

Finally, the strain of the composite film (ε^0) is found by the following

$$\varepsilon^0 = \frac{\sum_i \left(\frac{E_i}{1 - v_i}\right)\varepsilon_i t_i}{A_{11} + A_{12}}$$

$$A_{11} = A^{|}\sum_i t_i$$
$$A_{12} = B^{|}\sum_i t_i$$

where A_{11} and A_{12} are terns of the extensional stiffness matrix for the composite as defined in [6].

$$\varepsilon^0 = \frac{\left(\frac{E_1 t_1}{1-v_1}\right)\varepsilon_1 + \left(\frac{E_2 t_2}{1-v_2}\right)\varepsilon_2}{\left(\frac{E_1 t_1}{1-v_1}\right) + \left(\frac{E_2 t_2}{1-v_2}\right)}$$

-Finite Element Analysis (FEA)

Due to the approximate nature of the Strength of Materials solution given above, it was necessary to produce a numerical solution that could account for factors that were previously neglected. Such factors included edge effects and a thick plate (non-large aspect ratio) response.

The process of creating a finite element model (FEM) will be described in detail below. However, there was one important point that needed to be established from the outset, and that was the application of strain to the system. It was decided that the best approach would be to model the system by making an analogy with the thermal distortion of a bimetallic substance. In the thermal case, two different materials are bonded together at a fixed temperature, and are then subjected to a temperature change. Because of the varying thermal expansion coefficients of the two materials, a strain arises and the system deforms. The strain is simply equal to the product of the temperature change with the difference in thermal expansion coefficients.

-Zernike Polynomials

Zernike Polynomials [13] are a set of orthogonal polynomials on a unit circle that are often used to fit optical distortions. In this project, Zernike polynomials are used to fit the results of finite element analyses. Due to the symmetry of the problem at hand, only radially symmetric Zernike terms (especially focus) are expected to be found in the fits. In addition, the fits will determine if there are any significant higher order aberrations. The first six Zernike polynomials are shown below.

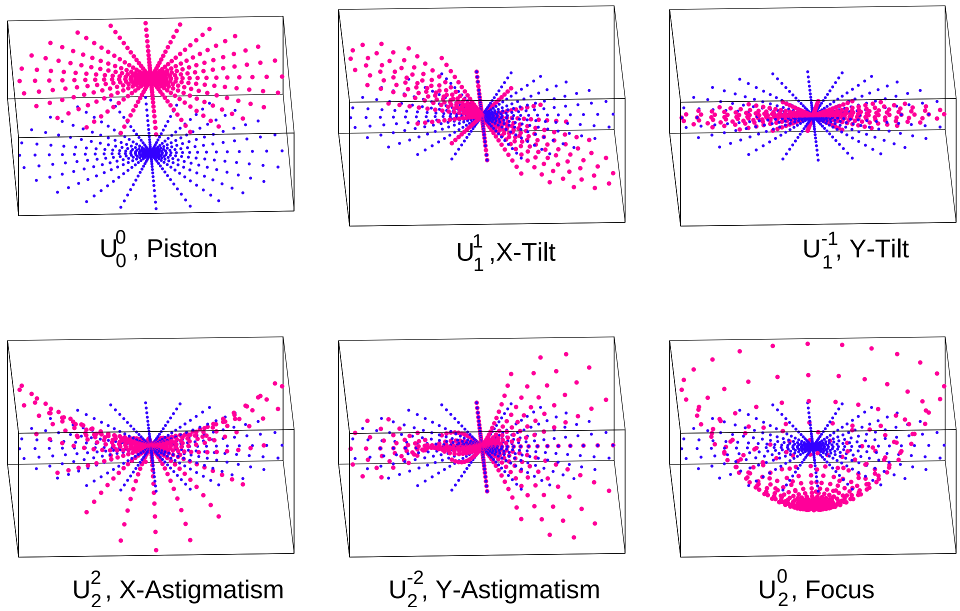

FIGURE 4. Plots of the First Six Zernike Polynomials and their Names.

Methods:

Distortion in LIGO optics was modeled using two approaches. The first approach was an analytical approach using the Strength of Materials formulation outlined in Section 2. The second approach was a finite element analysis done through use of *Structural Dynamics Research Corporation's* ***IDEAS*** computer simulation software [*8*]. Before beginning modeling of the LIGO cases, it was important to be sure that the analytical and finite element analyses produced near-identical results in an ideal case. To be sure of this, a "coupon" case was constructed.

-*Analytical Model-Coupon Case*

The Strength of Materials formulation was coded into ***Mathematica***, using the following parameters for the coupon and film.

TABLE 1. Coupon Parameters

Parameter	Value
Elastic modulus of substrate (Si)	130 GPa
Poisson's ratio of substrate (Si)	0.28
Substrate thickness	1 mm
Substrate/Film Diameter	7.62 cm
Elastic modulus of film (SiO_2)	73 GPa
Poisson's ratio of film (SiO_2)	0.17

Parameter	Value
Film Thickness	150 nm
Applied Strain	10^{-7}

Values for maximum deflection and curvature of the substrate were calculated and plotted.

-*Finite Element Model-Coupon Case*

There were five basic stages in the finite element analysis. They were coupon construction, meshing, boundary condition definition, model solution, and post processing of the results.

In designing the coupon, the physical parameters listed above were used. Then, the entire volume of the coupon was meshed using 4000 linear volume elements. The elements were defined so that they maintained the mechanical properties of the substrate listed in the above table. In addition, the thermal coefficient of expansion was set to zero. After this step, one surface of the coupon was meshed using 800 linear thin shell elements. The proper mechanical and physical properties for the *film* were entered, and a thermal expansion coefficient of 10^{-7} was set (this number was arbitrary since the only investigation being done was that of the consistency of the two models). Thus, the volume elements represented the substrate, and the shell elements represented the film.

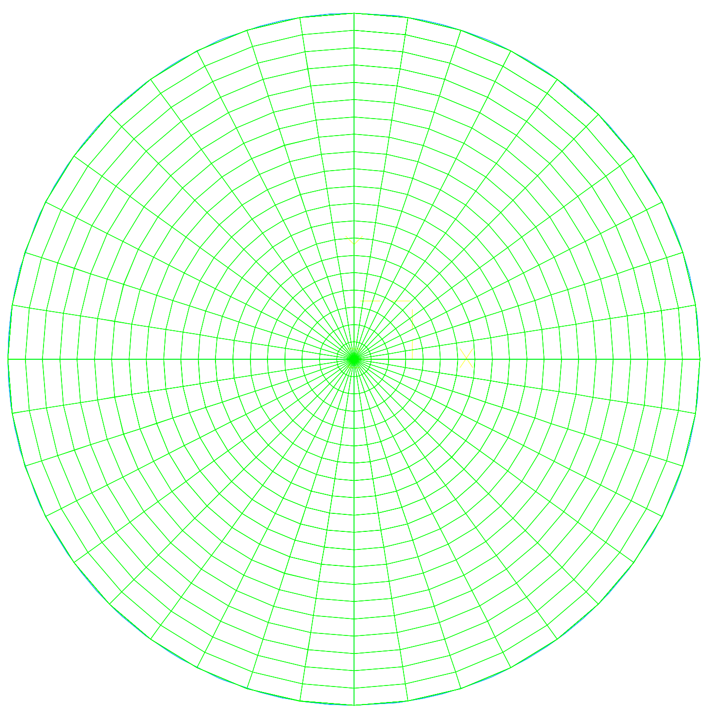

FIGURE 5. Finite Element Mesh of the Coupon

Defining the boundary conditions first called for placing restraints on the mesh. The restraints limit the degrees of freedom of the mesh, so it was important that they were carefully chosen. The cylindrical symmetry of the problem made it possible to define the restraints as shown below. These restraints make the problem kinematically stable (no rigid body motions).

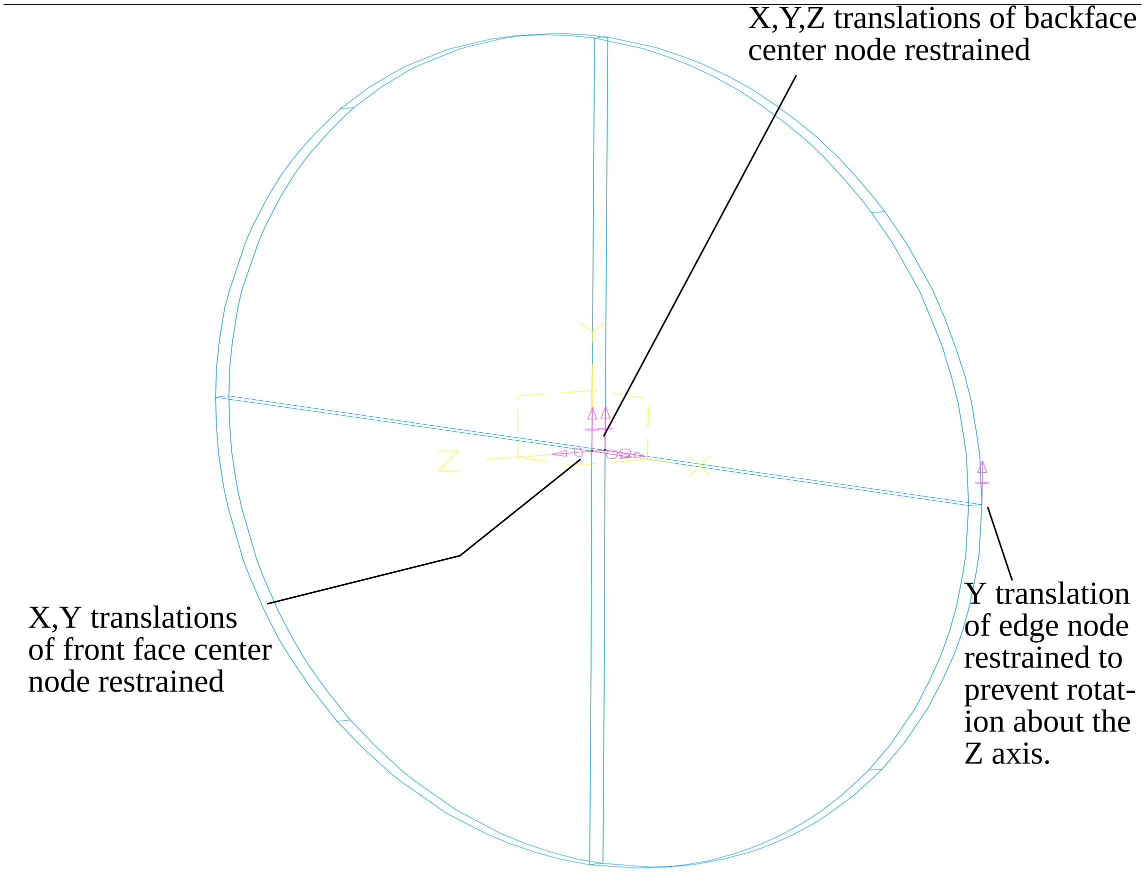

FIGURE 6. Restraint Set on Coupon

To complete the boundary condition set, a temperature change of one degree celsius was applied to the 4806 nodal points in the mesh. This temperature change, when combined with the thermal coefficient expansions of the substrate (volume mesh) and film (shell mesh) as described above constitutes a strain of $\Delta\alpha\Delta T = 10^{-7}$.

The linear static simulation was then run and the results of the analysis were read into a ***Mathematica*** module that fit the displacement results to Zernike polynomials. Zernikes up to 45th order were used to ensure small error (less than 0.1 percent). From the Zernike polynomials, substrate curvature and maximal deflection were calculated.

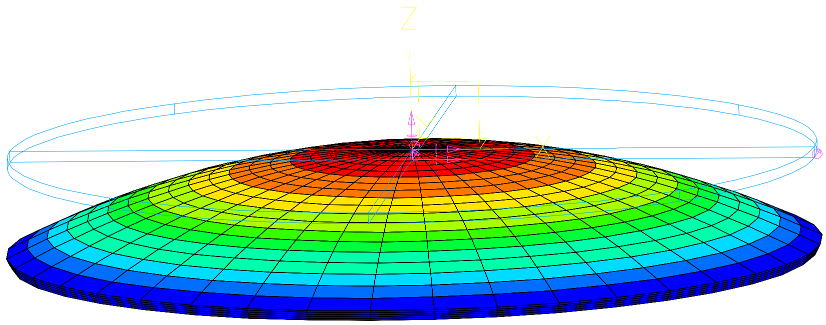

FIGURE 7. Finite Element Analysis Model of the Elastostatic Deformation of the Silicon Coupon. A strain of 10^{-7} was applied.

Three other finite element models for the coupon were created. The boundary conditions and method for meshing remained the same, but the mechanical properties of the film and substrate were changed. These models were created in order to show the consistency of the finite element and analytical models, as described below.

-Comparison to Analytical Model-Coupon Case

The finite element analysis results were compared to the results of the analytical model to show the consistency of the two approaches in the ideal case. This was done in two ways. The first was a direct comparison of displacement results for the coupon. The second was a plot of maximum displacement versus “effective biaxial modulus” for both the finite element and analytical models (in theory, such a graph should be linear). The results of the plots show that the finite element and analytical models agree very well in the thin plate situation.

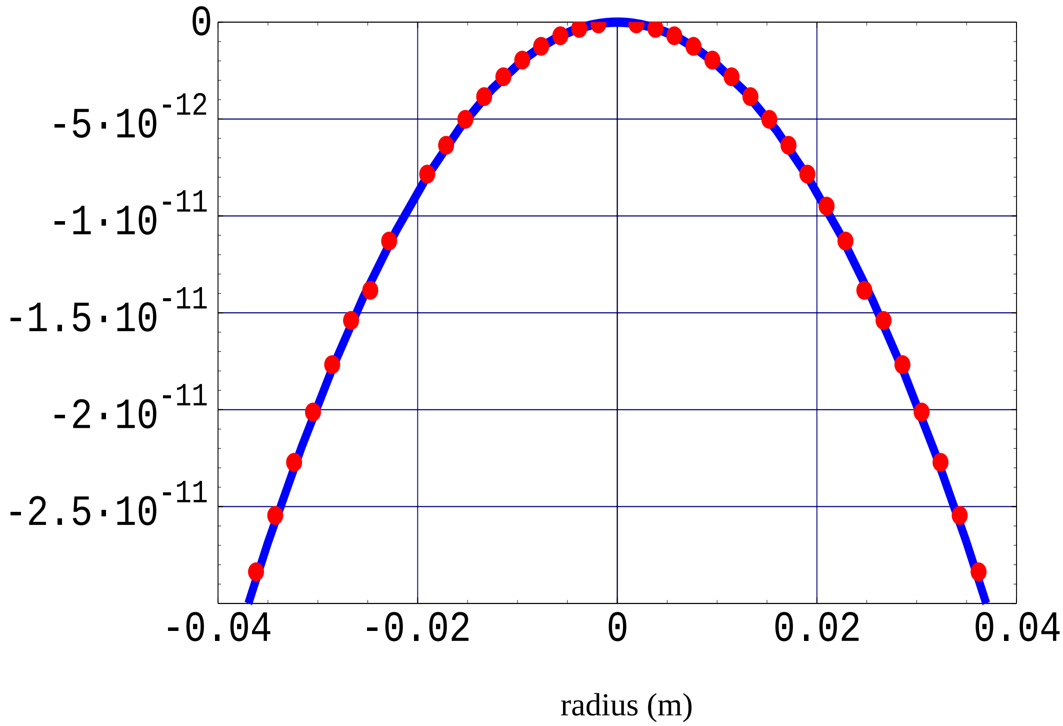

FIGURE 8. Elastostatic Front Surface Displacement (in m) along a diametrical cut for the Silicon Coupon. The curve gives the analytical solution, while the points correspond to data taken from the Finite Element Analysis. The applied strain was 10^{-7}.

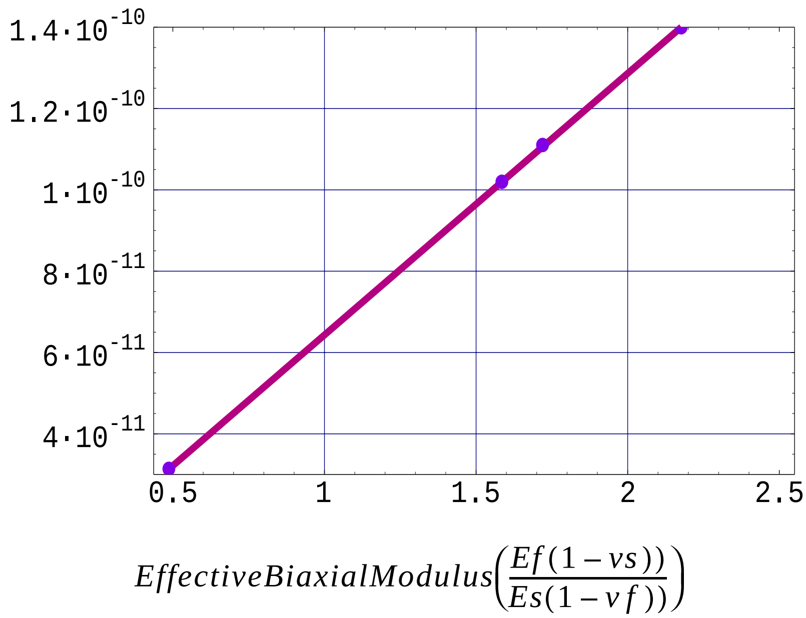

FIGURE 9. Graph of Deformation (Magnitude, in meters) versus the “Effective Biaxial Modulus” for the silicon coupon. The curve gives the theoretical relationship, while the points correspond to data taken from Finite Element Analyses.

-LIGO Core Optics

The analytical and finite element models were applied to the LIGO Core Optical Components (COC) using the physical parameters [9] compiled in Table 2. The terms HR coating and AR coating stand for high reflectance and antireflective coatings, respectively. Completed LIGO optics have an HR Coating on one face and an AR Coating on the opposite face.

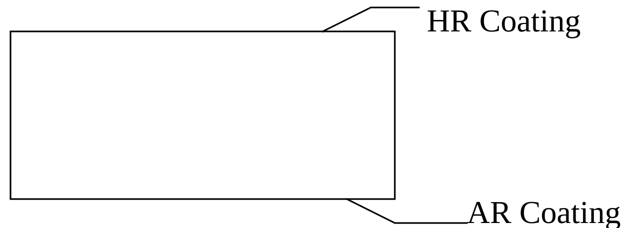

FIGURE 10. Profile of LIGO Optic showing locations of HR and AR Coatings

TABLE 2. Physical Properties of LIGO Core Optics

Parameter	End Test Mass (ETM)	Input Test Mass (ITM)	Beam Splitter (BS)	Recycling[a] Mirror
Thickness (m)	0.10	0.10	0.04	0.10
Diameter (m)	0.125	0.125	0.125	0.125
Coatings	40 Layer HR 2 Layer AR	16 Layer HR 2 Layer AR	4/7 Layer HR 2 Layer AR	14 Layer HR 2 Layer AR
Thickness of SiO_2 in HR Coating (μm)	5.32	2.128	0.532 (4 Layer) 1.064 (7 Layer)	1.862
Thickness of Ta_2O_5 in HR Coating (μm)	5.32	2.128	0.532 (4 Layer) 0.798 (7 Layer)	1.862
Total Thickness of HR Coating (μm)	10.64	4.256	1.064 (4 Layer) 1.862 (7 Layer)	3.724
Thickness of SiO_2 in AR Coating (μm)	0.1588	0.1588	0.1588	0.1588
Thickness of Ta_2O_5 in AR Coating (μm)	0.4841	0.4841	0.4841	0.4841
Total Thickness of AR Coating (μm)	0.6429	0.6429	0.6429	0.6429

Parameter	End Test Mass (ETM)	Input Test Mass (ITM)	Beam Splitter (BS)	Recycling[a] Mirror
Radius of Curvature (m)	7400	14540	inf	9890
Tolerance on Radius of Curvature	+/- 150	+145 -1000	>200 km, concave >720 km, convex	+500 -100

a. Due to the current tentativeness in the exact thicknesses of the coatings and the similarities between the Recycling Mirror and the Input Test Mass, separate models were not run for the Recycling Mirror.

Initial LIGO Optics will be made of Fused Silica, while a possible material for more advanced optics is Sapphire. By changing the mechanical properties of the substrate in the analytical and finite element models, analyses were run for both types of substrate material.

-Analytical Model-LIGO Optics

Few modifications had to be made to the previous ***Mathematica*** module to adapt it to LIGO COC (Core Optical Component) cases. The most important difference between these optics and the coupon (other than obvious parameters such as size and mechanical properties) is that these optics have coatings on both circular faces. This issue is resolved easily once it is seen that the strain in the coating on the other side of the optic (the Anti-Reflective (AR) Coated Face) will have a compensatory effect on the deflection and curvature of the side of the optic with the High-Reflectance (HR) Coating. Thus, the total curvature of the HR-coated face will equal the curvature that would be induced if it was the only coating minus the curvature that would be induced by an AR-coated optic.

Next, it was necessary to determine the mechanical properties and the proper strains that would exist in the HR and AR coatings (the coatings are composed of films made of two different materials, SiO_2 and Ta_2O_5). This required mechanical properties and stress values for the coatings, and the task proved to be non-trivial. As far as mechanical properties goes, it is important to realize that much of the data on mechanical properties of materials that is found in literature is for bulk materials. Thin films can have completely different microstructures (depending on the deposition process), however, and would thus have different properties. After much unsuccessful searching, it was decided that the SiO_2 coating would be given the mechanical properties of bulk SiO_2 (E=73 GPa and v=0.17). A somewhat ambiguous value that was found for the elastic modulus of Ta_2O_5 (E=140 GPa) was used [10], and a value was *assigned* for its Poisson's ratio (v=0.23). A literature search on stress values for ion beam sputtered SiO_2 and Ta_2O_5 coatings produced a range of stress values for the coatings. All of the stress values were in the 10^8 Pa range, but otherwise varied. Two particular stress values, 5.5×10^8 Pa for SiO_2 and 3.2×10^8 Pa for Ta_2O_5 were used [11]. From these stress values and the mechanical properties listed above, HR and AR mechanical properties and coating strains were calculated and the deformation of the optics (both fused silica and sapphire) was found. In particular, deflection was calculated in the optical zone, which is the central 8 cm diameter of the optic that receives nearly 65% (1-1/e) of the incoming laser beam.

Because so much guesswork had to be done in the selection of mechanical properties of the films, two more trials were done (for an ETM) using different values. Also, deflection values were calculated for an ETM for a range of stress values (for SiO_2 and Ta_2O_5). These results as well as the results of previous trials are contained in the next (*Results*) section.

Finally, due to the large degree of similarity between the recycling mirror and the input test mass, and because of the current tentativeness in the exact specifications for coating thicknesses, it was decided that separate models would not be run for the recycling mirror (radius of curvature changes would be calculated using ITM results).

-Finite Element Model-LIGO Optics

Most of the steps for constructing finite element models for the COC were the same as they were in the coupon case. The primary differences were designing properly-sized models and meshing these models so that they were coated on both circular faces. This meant that both faces of the optic were meshed with thin shell elements after the entire optic was meshed with volume elements. Each set of thin shell elements was given the proper physical and mechanical properties (as calculated from the above section).

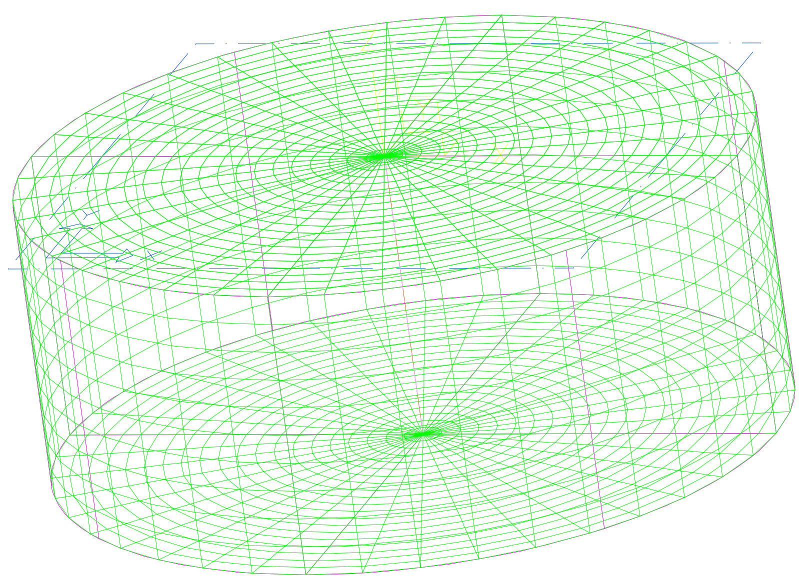

FIGURE 11. Finite Element Mesh of an End Test Mass

A few extra analyses were done for an ETM (both fused silica and sapphire) with different stress values so that a range of deflection values could be calculated.

As was done in the coupon case, the results of the FEM's were analyzed using the Zernike decomposition program. However, in this case, the fits were only done over the optical zone and a slightly larger (3 inch) radius. The reason for this was that the FEM's showed substantial edge effects for the optics, and it was difficult to produce fits that included such effects. After calculating optical zone deflections, radii of curvature values (for the deformed optics) were produced. The procedure for doing so was very similar to that discussed in section 1 (*Introduction*), except there were a couple of variations. The most important new point considered was that of the coating non-uniformity. Based upon experimental testing of single-layer coated optics, values for coating non-uniformity (as a function of mirror radius) due to the process of deposition (without considering intrinsic strain) were extrapolated [12]. The process of calculating the radius of curvature for a strained optic was as follows. First, a deflection value at the 3 inch radius for an undeformed optic was calculated using the nominal radius of curvature and the formula given previously. Due to the sensitivity of the calculations, the first order Taylor's approximation was not made. The value for the coating non-uniformity was then added (this value was given at the 3 inch radius, thus necessitating calculations to be done at that distance) to give the deflection for a coated but unstrained optic. Finally, the deflection value found in the FEA was subtracted to give an overall deflection. From this, the radius of curvature was recalculated. All of the results referred to here are listed in the next section.

Results:

Below is the finite element model for the deformation of a fused silica end test mass. The figure shows how deformation in the LIGO COC differs from the thin plate (coupon) case.

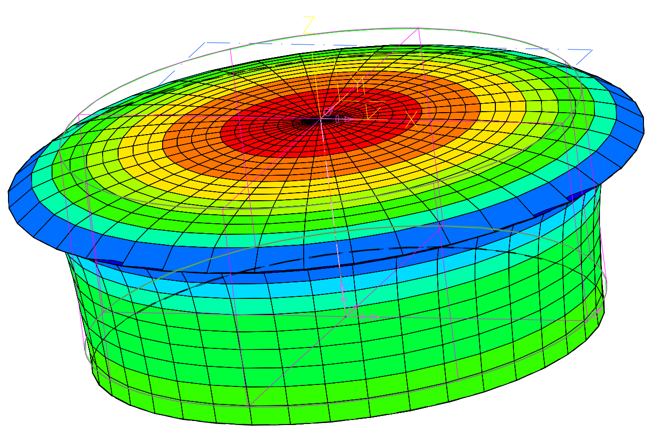

FIGURE 12. Finite Element Analysis Model of the Elastostatic Deformation of a Fused Silica End Test Mass. The applied strains were 10^{-6} for the HR Coating and $7.365*10^{-7}$ for the AR Coating.

Before listing tables of results for the various cases, a comparison is made between the analytical and finite element analyses for an End Test Mass. The graph below shows that there still is a good deal of agreement between the two models, but that the differences between the models are significant (the difference in optical zone deflection averaged about 15%). The differences are smaller in the beamsplitter cases, as the beamsplitter (with an aspect ratio of 6.25) more closely resembles a thin plate than the test masses.

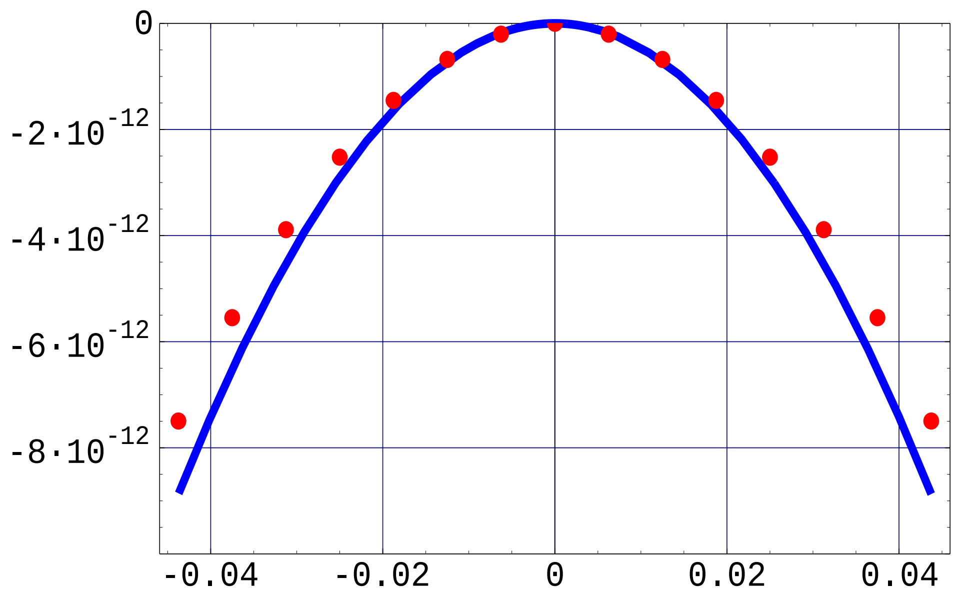

FIGURE 13. Elastostatic Front Surface Displacement (in the Optical Zone) along a linear cut for a Fused Silica End Test Mass. The curve gives the analytical solution, while the points correspond to data taken from the Finite Element Analysis. The applied strains were 10^{-6} for the HR Coating and $7.365*10^{-7}$ for the AR Coating.

The following tables give *unscaled* and then scaled deflection values for fused silica optics. The strains for HR and AR coatings that were previously calculated were not the values that were used in the initial FEM's. Rather, lesser values were initially applied, allowing those results to be scaled up as necessary (as long as the ratio of HR strain to AR strain is correct and remains constant, deformation scales linearly).

TABLE 3. Results for Fused Silica Optics(Unscaled)

Physical Quantity	ETM	ITM	BS 4 Layer	BS 7 Layer
t_{HR} (μm)	10.64	4.256	1.064	1.862
$t_{SUBSTRATE}$(mm)	100	100	40	40
E_{HR} (GPa)	106.5	106.5	106.5	101.71

Physical Quantity	ETM	ITM	BS 4 Layer	BS 7 Layer
$E_{SUBSTRATE}$ (GPa)	73.0	73.0	73.0	73.0
v_{HR}	0.21	0.21	0.21	0.206
$v_{SUBSTRATE}$	0.17	0.17	0.17	0.17
t_{AR} (μm)	0.6429	0.6429	0.6429	0.6429
E_{AR} (GPa)	123.45	123.45	123.45	123.45
v_{AR}	0.221	0.221	0.221	0.221
σ (SiO_2) (Pa)	$5.5*10^8$	$5.5*10^8$	$5.5*10^8$	$5.5*10^8$
σ (Ta_2O_5) (Pa)	$3.2*10^8$	$3.2*10^8$	$3.2*10^8$	$3.2*10^8$
Strain Applied (HR)	10^{-6}	10^{-6}	10^{-6}	$1.092*10^{-6}$
Strain Applied (AR)	$7.365*10^{-7}$	$7.365*10^{-7}$	$7.365*10^{-7}$	$7.365*10^{-7}$
Optical Zone Deflection w/o AR (Analytic) (pm) [a]	-7.826	-3.130	-4.891	-8.881
Optical Zone Deflection w/o AR (FEM) (pm)	-6.691	-2.678	-4.891	-8.875
Optical Zone Deflection w/ AR (Analytic) (pm)	-7.416	-2.721	-2.330	-6.321
Optical Zone Deflection w/ AR (FEM) (pm)	-6.228	-2.215	-2.334	-6.319

a. Optical Zone Deflection=Deflection at radius of 4 cm

TABLE 4. Scaled Results for Fused Silica Optics

Physical Quantity	ETM	ITM	BS 4 Layer	BS 7 Layer	Recycling Mirror
Optical Zone Deflection w/o AR (Analytic) (nm)	-25.24	-10.100	-15.77	-28.65	-10.100
Optical Zone Deflection w/o AR (FEM) (nm)	-21.58	-8.635	-15.77	-28.62	-8.635
Optical Zone Deflection w/ AR (Analytic) (nm)	-23.92	-8.774	-7.515	-20.39	-8.774
Optical Zone Deflection w/AR (FEM) (nm)	-20.85	-7.142	-7.528	-20.38	-7.142

Physical Quantity	ETM	ITM	BS 4 Layer	BS 7 Layer	Recycling Mirror
Coating Non-Uniformity (nm)[a]	12.2	4.89	1.22	2.14	4.89
Radius of Curvature (m)[a]	8730	16225	inf	inf	10529
Difference from Nominal Radius of Curvature (m)	1330	1685	-111.5 km	-40.41 km	752
Tolerance on Radius of Curvature	+/- 150	+145 -1000	>200 km, concave >720 km, convex		+500 -100

a. Coating Non-Uniformity, Radius of Curvature taken at a 3 inch (7.62 cm) radius

The following table, which was previously alluded to, shows the variation of deflection with differing mechanical properties for the film. As will be discussed in the following section (*Discussion*), the deflection appears to be nearly constant regardless of the properties of the film.

TABLE 5. Dependence of ETM (Fused Silica) Optical Zone Deflection on Mechanical Properties of the Coatings (Scaled)

Physical Quantity[a]	Case 1	Case 2	Case 3
E SiO_2 (GPa)	73.0	73.0	85.0
v SiO_2	0.17	0.17	0.21
E Ta_2O_5 (GPa)	140	290	290
v Ta_2O_5	0.23	0.25	0.25
Optical Zone Deflection, Analytical (nm)	-23.92	-23.91	-23.93

a. HR and AR Strains and physical parameters of the mirrors and coatings are the same as in Tables 3 and 4

Next, as stated previously, deflection and radii of curvature were calculated for a range of values for an End Test Mass with both HR and AR coatings.

TABLE 6. Range of Deflection Values for a Fused Silica End Test Mass (Scaled)

Physical Quantity	Case 1[a]	Case 2	Case 3	Minimum Deformation[b]	Maximum Deformation
σ (SiO_2) (Pa)	$5.50*10^8$	$1.83*10^8$	$9.00*10^8$	$1.00*10^8$	$9.99*10^8$
σ (Ta_2O_5)(Pa)	$3.20*10^8$	$1.07*10^8$	$4.50*10^8$	$1.00*10^8$	$9.99*10^8$
σ (HR Coating) (Pa)	$4.35*10^8$	$1.45*10^8$	$6.74*10^8$	$9.99*10^7$	$9.98*10^8$
σ (AR Coating) (Pa)	$3.76*10^8$	$1.26*10^8$	$5.61*10^8$	$1.00*10^8$	$9.99*10^8$
Optical Zone Deformation (Analytic) (nm)	-23.92	-7.97	-37.20	-5.45	-54.46
Optical Zone Deformation (FEM) (nm)	-20.85	-6.95	-32.44	-4.75	-47.47
Coating Non-Uniformity (nm)[c]	12.2	12.2	12.2	12.2	12.2
Radius of Curvature (m)[d]	8730	7629	10120	7496	12499
Difference from Nominal Radius of Curvature (m)	1330	229	2720	96	5099
Tolerance on Radius of Curvature	+/- 150				

a. Cases 1-3 use stress values similar to those found in literature
b. Minimum and Maximum Deformation values are found assuming that the stress values for SiO_2 and Ta_2O_5 are in the 10^8 Pa range
c. Coating Non-Uniformity taken at 3 inch radius
d. Radius of Curvature taken over a 3 inch radius

Tables 3,4, and 6 were repeated for sapphire optics.

TABLE 7. Results for Sapphire Optics (Unscaled)

Physical Quantity	ETM	ITM	BS 4 Layer	BS 7 Layer
t_{HR} (μm)	10.64	4.256	1.064	1.862

Physical Quantity	ETM	ITM	BS 4 Layer	BS 7 Layer
$t_{SUBSTRATE}$(mm)	100	100	40	40
E_{HR} (GPa)	106.5	106.5	106.5	101.71
$E_{SUBSTRATE}$ (GPa)	344.74	344.74	344.74	344.74
v_{HR}	0.21	0.21	0.21	0.206
$v_{SUBSTRATE}$	0.29	0.29	0.29	0.29
t_{AR} (μm)	0.6429	0.6429	0.6429	0.6429
E_{AR} (GPa)	123.45	123.45	123.45	123.45
v_{AR}	0.221	0.221	0.221	0.221
σ (SiO_2)	$5.5*10^8$	$5.5*10^8$	$5.5*10^8$	$5.5*10^8$
σ (Ta_2O_5)	$3.2*10^8$	$3.2*10^8$	$3.2*10^8$	$3.2*10^8$
Strain Applied (HR)	10^{-6}	10^{-6}	10^{-6}	$1.092*10^{-6}$
Strain Applied (AR)	$7.365*10^{-7}$	$7.365*10^{-7}$	$7.365*10^{-7}$	$7.365*10^{-7}$
Optical Zone Deflection w/o AR (Analytic) (pm)	-1.418	-0.5670	-0.8860	-1.609
Optical Zone Deflection w/o AR (FEM) (pm)	-1.200	-0.4800	-0.8860	-1.608
Optical Zone Deflection w/ AR (Analytic) (pm)	-1.343	-0.4928	-0.4221	-1.144
Optical Zone Deflection w/AR (FEM) (pm)	-1.115	-0.3956	-0.4229	-1.145

TABLE 8. Scaled Results for Sapphire Optics

Physical Quantity	ETM	ITM	BS 4 Layer	BS 7 Layer	Recycling Mirror
Optical Zone Deflection w/o AR (Analytic) (nm)	-4.572	-1.829	-2.857	-5.189	-1.829

Physical Quantity	ETM	ITM	BS 4 Layer	BS 7 Layer	Recycling Mirror
Optical Zone Deflection w/o AR (FEM) (nm)	-3.870	-1.548	-2.857	-5.186	-1.548
Optical Zone Deflection w/ AR (Analytic) (nm)	-4.332	-1.589	-1.361	-3.692	-1.589
Optical Zone Deflection w/AR (FEM) (nm)	-3.597	-1.276	-1.364	-3.692	-1.276
Coating Non-Uniformity (nm) [a]	12.2	4.89	1.22	2.14	4.89
Radius of Curvature (m)[b]	7412	14517	inf	inf	9879
Difference from Nominal Radius of Curvature (m)	12	-23	-1026 km	-258 km	-11

a. Coating Non-Uniformity taken at 3 inch radius
b. Radius of Curvature taken over a 3 inch radius

TABLE 9. Range of Deflection Values for a Sapphire End Test Mass (Scaled)

Physical Quantity	Case 1[a]	Case 2	Case 3	Minimum Deformation[b]	Maximum Deformation
σ (SiO_2) (Pa)	$5.50*10^8$	$1.83*10^8$	$9.00*10^8$	$1.00*10^8$	$9.99*10^8$
σ (Ta_2O_5)(Pa)	$3.20*10^8$	$1.07*10^8$	$4.50*10^8$	$1.00*10^8$	$9.99*10^8$
σ (HR Coating) (Pa)	$4.35*10^8$	$1.45*10^8$	$6.74*10^8$	$9.99*10^7$	$9.98*10^8$
σ (AR Coating) (Pa)	$3.76*10^8$	$1.26*10^8$	$5.61*10^8$	$1.00*10^8$	$9.99*10^8$
Optical Zone Deformation (Analytic) (nm)	-4.332	-1.444	-6.737	-0.9874	-9.864
Optical Zone Deformation (FEM) (nm)	-3.597	-1.199	-5.594	-0.8199	-8.190
Coating Non-Uniformity (nm)[c]	12.2	12.2	12.2	12.2	12.2

Physical Quantity	Case 1[a]	Case 2	Case 3	Minimum Deformation[b]	Maximum Deformation
Radius of Curvature (m)[d]	7435	7253	7556	7230	7746
Difference from Nominal Radius of Curvature (m)	35	-147	156	-170	346

a. Cases 1-3 use stress values similar to those found in literature
b. Minimum and Maximum Deformation values are found assuming that the stress values for SiO_2 and Ta_2O_5 are in the 10^8 Pa range
c. Coating Non-Uniformity taken at 3 inch radius
d. Radius of Curvature taken over a 3 inch radius

A summary table of the Zernike Fits for the fused silica optics is shown below. As expected, the asymmetric coefficients were much smaller (by orders of magnitude) than the symmetric terms. In addition, the focus term was larger by two orders of magnitude over the next largest term.

TABLE 10. Zernike Decomposition over the Optical Zone (r<4 cm)

No.	**U**	**Description/Eqn.**	**Amplitude (nm)**			
			ETM	**ITM**	**BS 4 Layer**	**BS 7 Layer**
6	U_2^0	Focus, $2\rho^2 - 1$	-10.41	-3.716	-3.916	-10.58
15	U_4^0	Spherical, $6\rho^4 - 6\rho^2 + 1$	0.0817	0.0309	0.0144	0.0395
28	U_6^0	$20\rho^6 - 30\rho^4 + 12\rho^2 - 1$	-0.0077	-0.0030	-0.0025	-0.0067
45	U_8^0	$70\rho^8 - 140\rho^6 + 90\rho^4 - 20\rho^2 + 1$	0.0307	0.0109	0.0102	0.0277

Discussion:

One important result shown above is that the deflection does not seem to vary (the small variations are probably numerical noise) with the mechanical properties of the film. After a bit of thought, this seems obvious in that the curvature (and therefore deflection) is a function of the film stress and elastic properties of the *substrate*, as given by the equation

$$K = \frac{6\sigma(1 - v_s)t_f}{E_s t_s^2}$$

Thus, equivalent results can be obtained despite uncertainties in the values for the mechanical properties of the film.

The deflection and radii of curvature values found for the deformed fused silica optics vary from acceptable to extremely large (when compared with what is tolerable, as indicated in Tables 4 and 6). In particular, the values found when stress values of $5.5*10^8$ Pa for SiO_2 and $3.2*10^8$ Pa for Ta_2O_5 were used are uniformly too large for all types of optics. However, other stress values, including those given in case 2 of Table 6 produce results that border on the acceptable

Coating strain produced deformations in sapphire optics that are almost uniformly well within the acceptable range of values. The reason for this is that sapphire has a biaxial modulus that is more than five times greater than that of fused silica, and deflection is inversely proportional to substrate biaxial modulus. It thus appears that coating strain induced distortion is not a significant effect when the substrate has as large an elastic modulus as sapphire does.

-Comparison to Experimental Results

Testing of full-size LIGO optics for radii of curvature changes before and after coating is still in its initial stage, so it is difficult to compare the results above with any real-life scenarios. However, a single test of a full-size End Test Mass with a 36 Layer HR Coating and a 2 Layer AR Coating has been done (the test produced a rough estimate of coating strain induced distortion by measuring the radius of curvature change between a coated and uncoated optic, and by using the extrapolated coating non-uniformity figure previously described). The results of this test show a deflection of -12 nm at the 3 inch radius, but the uncertainty in the measurement is -14 nm. Scaling to a 40 Layer HR Coating, this gives a deflection of around -13 nm with a similar uncertainty.

While the case 1 deflection at the 3 inch radius (approx. -75 nm) is certainly *much* larger than this experimental amount, the case 2 deflection at the 3 inch radius(approx. -25 nm) is within the uncertainty (note that the previous results tables give deflection values in the optical (4 cm radius) zone, but for the sake of comparison with experiment, values were calculated at the 3 inch radius as well).

-Further Remarks on Coating Strain Induced Distortion

The most important point to remember at this time is that these results and the experimental results discussed above are for *unannealed* coatings. In general, most coatings undergo a process of annealing in which much of the intrinsic stress is relieved. Annealing can reduce stress values greatly (>33 %) [15]. Thus, an annealed optic is likely to have a more tolerable radius of curvature. Before annealing the optics, however, it would be important to understand the process and how it might structurally affect the coatings (in particular, how it might change the uniformity and/or thickness of the coatings).

It is also important to realize that the formation of coating stress depends almost completely upon the deposition technique. Thus, the coating stress values published in literature might not be indicative of coating stress values in LIGO optics if the deposition techniques differ greatly.

Conclusions:

The analytical and finite element models provided some clarity regarding the problem of coating strain induced distortion in LIGO optics. They gave estimates for distortion in the optics and showed that it is a problem that needs to be reviewed carefully in the future. In particular, it is important that extensive tests be done (they are presently occurring) to better determine how great a factor coating strain induced distortion will be. In addition, the work shows that annealing will probably be an important process in completing an optic and should therefore carefully be studied to determine its effects.

Acknowledgments:

Thanks go to Dennis Coyne for spending a great deal of time helping me with the project regardless of how much other work he had. I also thank Robbie Vogt for investing much of his time organizing and overseeing the LIGO Summer Undergraduate Program. In addition, I would like to thank Stan Whitcomb and Garilynn Billingsley for their helpful discussions and input. Finally, I would like to express my appreciation for the SURF Program at Caltech and the work that it does in assisting undergraduates in their pursuit of research opportunities.

Bibliography:

[1] Nix, William D. ***Mechanical Properties of Thin Films.*** *Metallurgical Transactions A* Vol. 20A, November 1989, 2217-2245.

[2] Windischmann, Henry. ***Intrinsic Stress in Sputter-Deposited Thin Films.*** *Critical Reviews in Solid State and Materials Science.* Vol. 17 (6), 1992, 547-596.

[3] Stoney, G.Gerald ***The Tension of Metallic Films deposited by Electrolysis.*** *Proceedings of the Royal Society of London, Series A.* Vol 82, 1909, 172-175.

[4] Hoffman, R.W. ***The Mechanical Properties of Thin Condensed Films.*** *Physics of Thin Films.* Vol 3, 1966, 211-270.

[5] Townsend, P. H., Barnett, D. M, and T.A. Brunner ***Elastic Relationships in Layered Composite Media With Approximation for the Case of Thin Films on a Thick Substrate.*** *Journal of Applied Physics.* Vol. 62 (11), December 1, 1987, 4438-4444.

[6] Jones. **Mechanics of Composite Materials**. Scripta Book Company, 1975

[7] Wolfram, S. ***Mathematica: A System for Doing Mathematics by Computer****, version 3.0* Addison Wesley Publishing Co.

[8] ***I-DEAS Master Series 4.*** *Structural Dynamics Research Corporation*

[9] Kells, William ***Core Optics Components Requirements (1064 nm).*** *LIGO E950090-04D.* 8/7/96.

[10] Martin, P.J., Bendavid, A., et al. ***Mechanical and Optical Properties of Thin Films of Tantalum Oxide Deposited by Ion-Assisted Deposition.*** *Thin Films: Stresses and Mechanical Properties IV* Proceedings of the symposium held from April 12-16, 1993.

[11] Cevro, M. ***Ion Beam Sputtering of $(Ta_2O_5)_x$-$(SiO_2)_{1-x}$ Composite Thin Films.*** *Thin Solid Films.* Vol 258, 1995, 91-103.

[12] Camp, J. ***Core Optics Components.*** *NSF Technical Review of the LIGO Project, 15-17 April 1997* LIGO-G970070-00-M

[13] Born and Wolf. **Principles of Optics, 6th Edition**. Pergamon Press, 1980.

[14] LIGO Core Optics Specifications

Input Test Mass E960093-A

End Test Mass E960102-A

Beam Splitter E960100-A

Recycling Mirror E960092-A

[15] Information provided by REO